PERGAMON

Journal of Structural Geology 26 (2004) 127–141

JOURNAL OF STRUCTURAL GEOLOGY

www.elsevier.com/locate/jsg

Intra-granular strains and grain boundary morphologies of dynamically recrystallized quartz aggregates in a mylonite

Osamu Nishikawa[a,*], Kazuto Saiki[b], Hans-Rudolf Wenk[c]

[a]*Institute for Study of the Earth Interior, Okayama University, Misasa Tottori-Ken, Japan*
[b]*Research Institute of Materials and Resources, Faculty of Engineering and Resource Science, Akita University, Akita, Japan*
[c]*Department of Earth and Planetary Science, University of California, Berkeley, CA 94720, USA*

Received 17 June 2002; received in revised form 5 April 2003; accepted 28 April 2003

Abstract

Dynamic recrystallization process has been investigated by analyzing intra-granular strains and grain boundary morphologies of sheared quartz aggregates deformed under high greenschist facies condition collected from the Hatagawa mylonite zone in northeast Japan. Microstructural features indicate pervasive operation of both subgrain rotation and grain boundary migration. The grains favorably oriented for operation of $\{10\bar{1}1\}\langle 11\bar{2}0\rangle$ and $\{10\bar{1}0\}\langle 11\bar{2}0\rangle$ slip systems tend to have small mean intra-granular misorientations (less than 3°) and occupy a large volume in the aggregate. Grains favorably oriented for $(0001)\langle 11\bar{2}0\rangle$ slip show large intra-granular misorientations, often exceeding 10°, and are often isolated as thin layers and equant small grains between those favorably oriented for prism$\langle a\rangle$ and rhomb$\langle a\rangle$ slip. The energies of subgrain boundary developed in the latter grains are estimated to be about 0.28 J m^{-2}, and are 1.5–2 times larger than the former. The morphological features of grain boundaries were well described by means of the curvature distribution along the boundary. The serration of grain boundaries is controlled by the misorientation and spacing of subgrain boundaries developed in the grain. We have demonstrated that serrated grain boundaries have a common asymmetric feature in the curvature distribution and this morphological feature can be used for the determination of direction of the grain boundary migration.

Keywords: Dynamic recrystallization; Strain; Misorientation; Grain boundary; Curvature distribution; Quartz

1. Introduction

During deformation of the Earth's crust at metamorphic conditions, strain energies stored in crystals are mostly released through dynamic recrystallization, which accommodate a large amount of strain without strain hardening. Many studies have been performed to investigate the dynamic recrystallization mechanisms in rock forming minerals (e.g. Hobbs, 1968; Poirier and Nicolas, 1975; Urai et al., 1986; Drury and Urai, 1990; Lloyd and Freeman, 1991, 1994; Gleason et al., 1993; Herwegh and Handy, 1996; Pauli et al., 1996; Herwegh et al., 1997; Trimby et al., 1998; Takeshita et al., 1999; Nishikawa and Takeshita, 2000). The driving force of dynamic recrystallization is thought to be a gradient of strain energy across boundaries (e.g. Bocher and Jonas, 1999). Strain free grains preferentially grow at the expense of highly strained grains, which changes microstructures and average crystallographic orientations rapidly in a steady state. Therefore, the strain accommodation process and grain growth are essential in dynamic recrystallization, and are considered to control the evolution of microstructure and texture, and also deformation behaviors of minerals (e.g. de Bresser et al., 1998, 2000).

The magnitude of strain energy stored in a grain depends on the configuration of dislocations (e.g. Humphreys and Hatherly, 1995; Hughes, 1999). Pile-up of dislocations, which typically develop in low temperature deformation, generates the highest magnitude of strain energy. On the other hand, under conditions where subgrain rotation processes effectively operate, dislocations are rearranged into subgrain boundaries resulting in reduction of bulk strain

* Corresponding author. Present address: Institute of Earth Sciences, Faculty of Science, Kanazawa University, Kakuma, Kanazawa, Japan. Tel.: +81-76-264-5723; fax: +81-76-264-5746.
E-mail address: nisikawa@earth.s.kanazawa-u.ac.jp (O. Nishikawa).

0191-8141/03/$ - see front matter © 2003 Elsevier Ltd. All rights reserved.
doi:10.1016/S0191-8141(03)00082-8

energy and simultaneously in a heterogeneous energy distribution in a grain. Under such conditions not only single dislocations, but also subgrain boundaries contribute to the stored strain energy (e.g. Jones, 1978; Humphreys and Hatherly, 1995; Doherty, 1997). In deformation experiments of metals up to several ten percents of strain, it has been reported that mean misorientation and spacing of subgrain boundaries depend on the amount of imposed strain and crystallographic orientation (e.g. Bailey and Hirsch, 1962; Dillamore et al., 1972; Doherty, 1974; Sakai and Ohashi, 1990; Humphreys and Hatherly, 1995; Hughes et al., 1998; Hughes, 1999). However, there are few studies that investigate differences in the mean misorientation and spacing of subgrain boundaries between newly growing and consumed grains in deformed rocks (e.g. Wheeler et al., 2001).

Serrated grain boundaries are often observed in polycrystals deformed by dislocation creep. The shape of serrated grain boundaries contains a lot of information about grain boundary migration processes and the nature of intra-granular strain. Several authors have attempted to characterize shapes of grain boundaries by means of Fourier spectra (Toriumi, 1989) and fractal dimension (Hornborgen, 1987; Tanaka and Iizuka, 1991; Kruhl and Nega, 1996; Takahashi et al., 1998). However, the shape parameters proposed by the above studies do not take into account processes operating on grain boundaries like diffusion, grain boundary migration, grain boundary sliding and subgrain rotation recrystallization. It is difficult to represent a natural irregular boundary shape with only a few bulk parameters. The curvature distribution analysis is one of the methods that quantitatively characterize the morphological features of grain boundaries. Saiki (1997) developed software for the measurement of boundary curvature and demonstrated its validity by applying it to an analysis of the rounding process of minerals. Individual curvature at any specific point on a boundary can be examined with this method. Therefore it is expected to extract morphological features accurately, even from boundaries with complicated shapes, and contribute to a better understanding of the grain boundary migration process.

In order to clarify the dynamic recrystallization process under conditions where both subgrain rotation and grain boundary migration operate pervasively, we studied sheared quartz aggregates deformed under high greenschist facies conditions. Firstly textures and microstructures in the aggregate were investigated to establish deformation conditions. Secondly, the degree and spatial distribution of strain stored in grains was estimated, based on dislocation density, the misorientation and spacing of subgrain boundaries. Grain boundary morphology was also analyzed from the viewpoint of the curvature distribution, and the controlling factors of the morphology and the grain boundary migration process are discussed.

2. Sample description

A mylonite sample was collected from an outcrop of the Kunimiyama granodiorite (Kubo et al., 1990) along Uketo-gawa river in the Hatagawa shear zone (Watanabe et al., 1953), trending NNW–SSE with approximately 1 km in width in the eastern margin of the Abukuma Mountains, NE Japan (Fig. 1). The Hatagawa shear zone, which separates the South Kitakami belt and the Abukuma belt, was estimated to have undergone 60 km of sinistral lateral movement (Otsuki and Ehiro, 1992). The age of intrusion of granotoids, exposed in the shear zone, is thought to be Cretaceous. Field evidence revealed that the Hatagawa shear zone had been already active before the intrusion events ceased (e.g. Kubo et al., 1990). The Kunimiyama granodiorite in this area mainly consists of quartz, plagioclase, K-feldspar, hornblende and magnetite, with secondary chlorite and epidote.

Detailed analyses on deformation structures and quartz *c*-axis lattice preferred orientation (LPO) have been performed by Koshiya (1987, 1988), Shigematsu and Yamagishi (2002) and Tsurumi et al. (2003). In the rocks

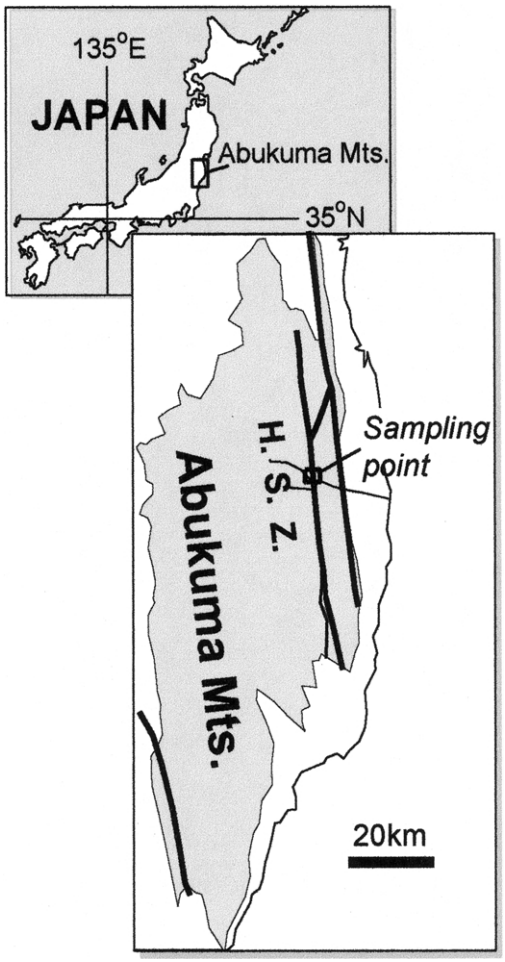

Fig. 1. Maps showing sample locality. H.S.Z.: Hatagawa Shear Zone. Shaded area in the large map denotes the area where Pre-Tertiary rocks are exposed.

around the sampling area, steeply dipping mylonitic foliations and stretching lineations parallel to the trend of the shear zone are developed. Asymmetric microstructures such as $S-C$ fabric, pressure shadow morphologies, shear bands and LPO indicate a sinistral sense of shear. The Y-point maximum (maximum in the intermediate strain direction) and asymmetric single girdle c-axis LPO patterns have been reported in this area. The former type dominantly develops in the eastern part of the shear zone, whereas the latter is found dominantly in the western part. The sampling locality for this study is at the eastern margin of the western part.

We have defined an orthogonal sample coordinate system such that X is parallel to the stretching lineation, Z is normal to the foliation plane, and Y is normal to the lineation and parallel to the foliation plane. All the observations were carried out on XZ thin sections. Clusters of quartz grains are flattened into 1–3 mm thick and 10–20 mm wide regions. These clusters are often connected forming penetrative networks of quartz aggregates. The studied quartz aggregates correspond to *microstructure A,* described as one of the representative microstructures by Shigematsu and Yamagishi (2002). It consists of coarse ribbon and small equant grains (Fig. 2). Ribbon grains, whose mean diameters and aspect ratios are 495 μm and 8.7, respectively, are oriented with their long axes parallel to X, forming banding structures. Fine equant grains with 11.1 μm mean diameter and 2.1 mean aspect ratio tend to prevail in highly strained portions, and seem to have been recrystallized from ribbon grains. Their long axes are oriented obliquely to the foliation, defining the S plane of $S-C$ structures (Lister and Snoke, 1984). Judging from the similarity of the microstructures of the present sample with those described by Stipp et al. (2002a,b) for a subgrain rotation regime, the studied sample probably deformed under middle to higher greenschist facies conditions.

3. Analytical procedures

3.1. Texture analysis using SEM–EBSP (electron back scatter pattern) system

For the texture analysis, a SEM–EBSP system (LEO-430 SEM) at the University of California, Berkeley was used at 10 kV accelerating voltage. The system contains a purely digital CCD camera. SEM functions, camera, as well as image processing, are controlled by the software SEMTEX (Wenk et al., 1999). The sample movements were made by stage translation with 0.05–0.1 mm step increments in X and 0.01 mm in Z directions. The crystallographic orientation of each diffraction image was determined by the CHANNEL + and partly CHANNEL5 software, produced by HKL Technology. Simulated and observed Kikuchi bands were compared in manual mode to confirm the correctness of indexing, particularly with respect to the hexagonal pseudo-symmetry of trigonal α-quartz.

The output orientation data are expressed by three Euler angles (Bunge, 1965). Multiplying three Euler rotations expressed in matrix form, they can be converted to a 3×3 orientation matrix for one grain $\boldsymbol{A}$, of which the 1st, 2nd and 3rd rows are, respectively, direction cosines of a^* (a direction in the reciprocal lattice which is normal to $(10\bar{1}0)$ in real lattice), a- and c-axes of the grain. The misorientation between two measurement points is expressed by a misorientation matrix $\boldsymbol{M}$, which relates $\boldsymbol{A}$ to the orientation matrix for second grain $\boldsymbol{B}$ as $\boldsymbol{AM} = \boldsymbol{B}$. The misorientation angle θ can be calculated by using the following relation: $tr\boldsymbol{M} = 1 + 2\cos\theta$, where tr is the trace of the matrix. The rotation axis of the misorientation can be obtained by calculating the Eigen-vector of $\boldsymbol{M}$ when the Eigen-value equals one. For the case of trigonal symmetry, there are six symmetrically equivalent axis and angle pairs of misorientations expressing a relation between two crystal lattice orientations. In accordance with previous workers (e.g. Randle, 1993), we chose the axis–angle pair with the smallest misorientation angle θ. The error of the measurement is generally about 1°.

Misorientations between neighboring measurement points in a grain were calculated for ribbon grains. The distance between measurement points influences the mean value of misorientations (e.g. Yoshizawa et al., 1995; Trozschel et al., 1997; Mino et al., 2000). If it is smaller than the spacing of subgrain boundaries, the mean misorientation obtained tends to be underestimated. On the other hand, if the spacing is much larger, the misorientation value may reflect a structure with a large characteristic length such as a kink band rather than a subgrain boundary. In this study, we adopted a 0.01 mm step increment. As described later, this value is slightly larger than the mean subgrain size developed in grains. In this analysis, we calculated misorientations not only in single ribbon grains, but also in 'ribbon domain', which all consist of fine grains of similar crystallographic orientation but misorientations exceeding 15°. The domains can be considered to have been originally one single ribbon grain.

3.2. Microstructural observation and misorientation analysis by TEM (transmission electron microscope)

Observation of dislocation substructures and determination of misorientations across subgrain boundaries were performed with a TEM (JEOL JEM-2000EX) at Hiroshima University, using an accelerating voltage of 120 kV and a double tilt specimen holder. The observations were carried out under two-beam conditions. The Burgers vectors of dislocations were determined using the invisibility criteria (e.g. McLaren, 1991). For misorientation analysis, we determined crystallographic orientations by TEM in the following way. By tilting the specimen, a low index lattice plane like (0001) or $\{11\bar{2}0\}$ was brought normal to the beam

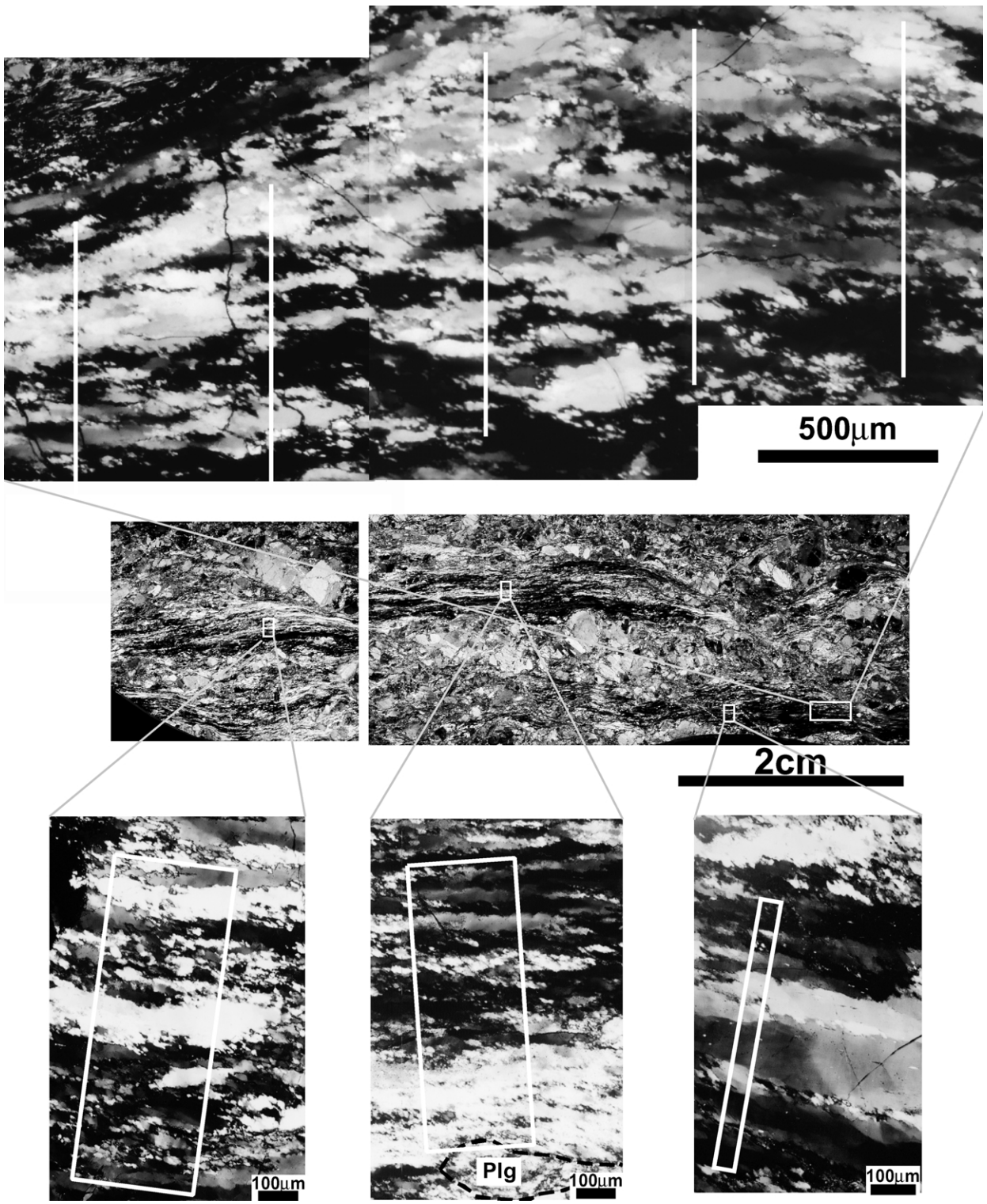

Fig. 2. Optical micrographs (crossed polarizers) of the studied quartz aggregates in a mylonite collected from the Hatagawa shear zone. Measurement lines and areas for crystallographic orientations by SEM–EBSP are marked by white lines and insets. Plg.: plagioclase porphyroclast.

direction to obtain a hexagonal or orthogonal diffraction pattern. We can uniquely determine the crystallographic orientation analyzing the diffraction pattern recorded on the film and reading rotation angles of the specimen holder. The accuracy of measurement for this method is 2–3°. For the subgrain boundaries with very small misorientation (2° >), the misorientation angles were determined by the method of Mawer and Fitz Gerald (1993). Diffraction patterns from both sides of a boundary were recorded simultaneously on a single photograph under the condition that a low index plane

of one side was oriented exactly normal to the beam direction. Analyzed quartz crystals were effectively treated as hexagonal in this method, because trigonality could not be identified with TEM diffraction intensities in this orientation.

3.3. Grain boundary shape analysis

We performed curvature distribution analysis for serrated grain boundaries between W- and B-grains with the following procedures: (1) tracing the boundary from a binary optical image of a grain, (2) thinning out pixels of the boundary trace for smoothing the curve, (3) interpolating between pixels by a cubic parametric spline, (4) assigning a set of points on the boundary trace with equal interval, and (5) calculating curvature of each point. Processes (2)–(5) were carried out using the Curvature Profiler (C-pro) software (Saiki, 1997), and the algorithm is described briefly. The trace of the grain boundary is expressed by two sets of cubic functions; $x = f(t)$ and $y = g(t)$. For interpolation by the cubic spline function, it must satisfy the conditions that the first and second derivatives are continuous across the boundary between the two intervals $(t_{j-1},\ t_j)$ and $(t_j,\ t_{j+1})$ $(0 < t_1 < t_2 < \ldots < t_n = 1)$. This restriction fixes a unique cubic function for each interval. Curvature at any point on the grain boundary trace can be calculated using the following equation:

$$\kappa = (y''x' - x''y')/(x'2 + y'2)^{1.5} \quad (1)$$

In this study, the points for the curvature calculation on the boundary traces were set at an interval of 0.75 μm. Since the photomicrographic images of grain boundaries are sometimes fuzzy and it is difficult to recognize the correct boundary lines, a threshold is needed for the binary process. We measured high angle grain boundaries with high brightness contrast across boundaries. The brightness in the image around boundary between bright and dark grains represents bimodal distributions. Therefore the threshold was chosen at the bottom between two peaks in the brightness distribution.

4. Results

4.1. Lattice preferred orientations (LPOs)

The *c*-axis [0001] LPO of the studied sample, measured by EBSP, exhibits an asymmetric single girdle pattern (Fig. 3a and b), which consists of a half small circle around the *Z* direction (W in Fig. 3b) and a cross girdle normal to the *X* direction (B in Fig. 3b). It has been suggested that the small circle component of *c*-axis LPO pattern of a sheared quartzite tends to asymmetrically distribute about the foliation pole (*Z*), with the greater concentration in the sense of shear (e.g. Garcia Celma, 1982; Dell'Angelo and Tullis, 1989; Wenk, 1994; Tomé and Wenk, 1999). In the studied sample, the shear sense inferred from the asymmetry of the pattern is sinistral (with *XY* as shear plane), in accordance with asymmetric microstructures. A remarkable feature of this pole figure is the fairly strong two maxima in the cross girdle component (B) and relatively weak small circle components (W). Similar *c*-axis LPOs with split maxima in the cross girdle have been reported frequently in this area (Koshiya, 1987, 1988; Shigematsu and Yamagishi, 2002; Tsurumi et al., 2003), and therefore the *c*-axis LPO pattern of Fig. 3a and b can be regarded as representative. The *a*-axis $\langle 11\bar{2}0\rangle$ LPO has six distinct maxima showing a hexagonal symmetric pattern. One of these maxima lies near the *X* direction (Fig. 3c), corresponding well with Wenk (1994, fig. 19a). The rhombs $r\{10\bar{1}1\}$ and $z\{01\bar{1}1\}$ poles, respectively, concentrated into single crystal orientations and show complementary LPO patterns (Fig. 3d and e). This suggests that the two rhombs did not operate as equivalent slip systems or that mechanical Dauphiné twinning determined the corresponding orientation variant.

The LPO patterns suggest that the grains composing the cross girdle in the *c*-axis pole figure (Fig. 4a and b) are optimally oriented for single slip on rhomb$\{1011\}$and prism$\{10\bar{1}0\}$, and those composing the small girdle (Fig. 4c) are optimally oriented for basal(0001) slip, in the $\langle a\rangle$ direction, assuming simple shear on the *XY* plane with *X* as shear direction. The intensities of orientation components in the pole figures reflect their area fractions rather than numbers of grains. Accordingly, it is evident from features of the *c*-axis pole figure that the grains favorably oriented for prism$\langle a\rangle$ and rhomb$\langle a\rangle$ slips occupy large volume fraction and those oriented for basal$\langle a\rangle$ slip are subordinate in the present sample. The grains favorably oriented for basal$\langle a\rangle$ are often isolated as thin layers and equant small grains between those favorably oriented for prism$\langle a\rangle$ and rhomb$\langle a\rangle$ slips. In this paper, we hereafter refer to the grains favorably oriented for prism$\langle a\rangle$ and rhomb$\langle a\rangle$ slip as B-grains, which appear dark gray to black in the *XZ* section, and those oriented for basal$\langle a\rangle$ slip as W-grains, which appear as light gray to white (Fig. 2).

The *c*-axis LPO in the present sample is intermediate between an asymmetric single girdle and a *Y*-point maximum pattern. It has been reported that the fabric transition from single girdle to *Y*-point maximum occurs at the transition from higher greenschist to lower amphibolite facies conditions (e.g. Takeshita and Wenk, 1988). Consequently, the deformation condition inferred from the LPO patterns is consistent with that from microstructural evidence mentioned above.

4.2. Dislocation substructures

Many dislocations are approximately parallel to $\{10\bar{1}1\}$ and $\{10\bar{1}0\}$, and dislocations parallel to (0001) are also observed in W-grains (Table 1, Fig. 5a). In two beam

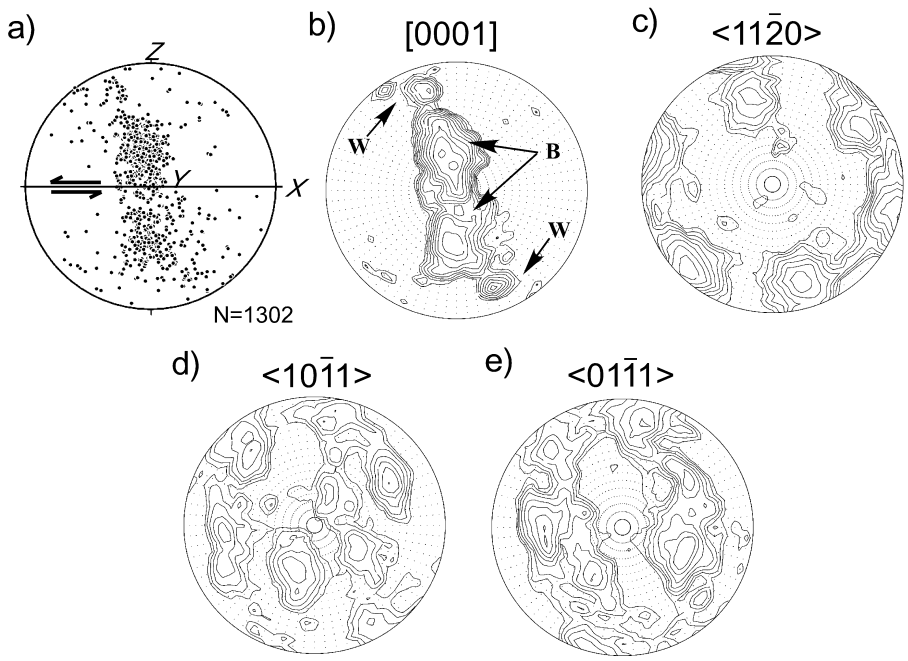

Fig. 3. Pole figures of crystallographic orientations for studied quartz aggregates, measured by EBSP (1302 grains). Lower hemisphere, equal area projection. (a) Single orientation plot for c[0001]. (b) Contoured pole figure of (a). B and W denote the orientation components of the B- and W-grains, respectively. (c) $a\langle 11\bar{2}0\rangle$, (d) r-pole$\langle 10\bar{1}1\rangle$ and (e) z-pole$\langle 01\bar{1}1\rangle$. Contours are at 0.5, 0.7, 1, 1.4, 2, 2.8, 4, 5.6, 8, 11.3, 16, 22.6, 32, 45 and 25 multiples of random distribution (m.r.d). Areas below 1 m.r.d are dotted. Contour pole figures were drawn by the BEARTEX software (Wenk et al., 1997, 1999).

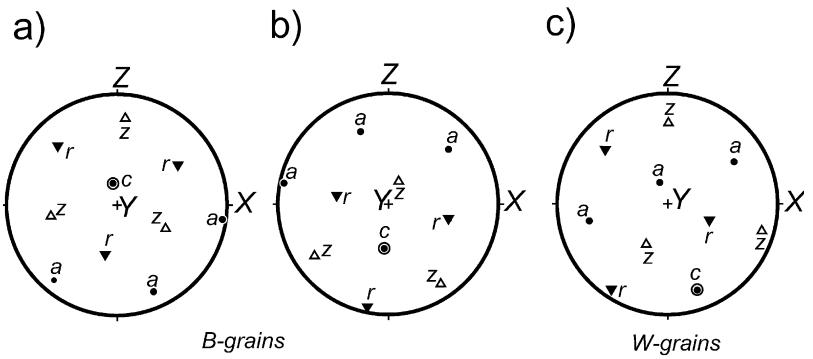

Fig. 4. The idealized single crystal orientations representing three major orientation components in the present sample. (a) and (b) B-grains, (c) W-grains. c, a, r and z denote c-axis, a-axes, and poles of positive and negative rhomb orientations, respectively.

Table 1
Dislocation densities and distribution patterns on the photomicrographs of TEM. W: W-grain which is favorably oriented for $(0001)\langle 11\bar{2}0\rangle$ (basal$\langle a\rangle$) slip, B: B-grain which is favorably oriented for prism$\{10\bar{1}0\}\langle a\rangle$ and rhomb$\{10\bar{1}1\}\langle a\rangle$ slips

Samples	Grains	Dislocation density (cm^{-2})	Distribution pattern of dislocations
Qz-s4-1	W	7.3×10^8	Dominantly parallel to $\{10\bar{1}1\}$, subparallel to (0001)
Qz-s4-3	W	6.1×10^8	Dominantly parallel to $\{10\bar{1}1\}$, subordinately $\{10\bar{1}0\}$
Qz-s4-5	B	4.5×10^8	Apparently random distribution
Qz-s4-7	B	3.1×10^8	Parallel to $\{10\bar{1}1\}$ and $\{10\bar{1}0\}$
Qz-s4-9	B	6.0×10^8	Very high angle to (0001)
Qz-s4-10	B	7.2×10^8	Very high angle to (0001)
Qz-s4-11	B	4.0×10^8	Mostly parallel to $\{10\bar{1}1\}$
Qz-s4-13	W	3.8×10^8	Apparently random distribution
Qz-s4-14	B	4.7×10^8	Both high and low angle to (0001)
Qz-s4-15	W	7.8×10^8	Dominantly parallel to $\{10\bar{1}1\}$, subordinately (0001)
Qz-s4-17	B	6.9×10^8	Mostly parallel to $\{10\bar{1}1\}$

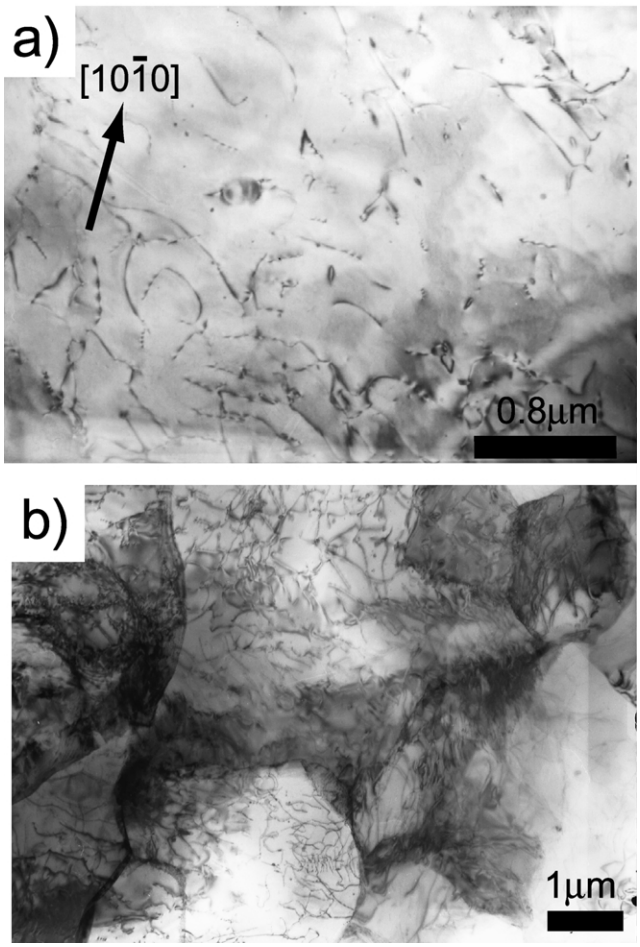

Fig. 5. TEM bright field image in a W-grain. (a) Many dislocations show an obliquity of about 52° and parallel to the prism(10$\bar{1}$0) plane. (b) Subgains developed in a grain.

conditions, almost all dislocations are in strong contrast for the reflection $g = 10\bar{1}1$, and have zero or very weak contrast for the reflection $g = 0003$, consistent with a Burgers vector $b = \langle a \rangle$. Therefore, rhomb$\langle a \rangle$ and prism$\langle a \rangle$ are suggested as dominant slip systems. The basal$\langle a \rangle$ slip system seems to have also operated in W-grains. This observation is consistent with the inference from the LPO patterns (Figs. 3 and 4).

Mean free dislocation densities in the present sample are generally ranging from 3.1 to 7.8×10^8 cm^{-2}, and no significant differences exceeding heterogeneity observed in a single grain are found among differently oriented grains (Table 1). Subgrains are pervasively developed in all the grains (Fig. 5b). Their sizes are approximately 5.7 μm in W-grains and 5.8 μm in B-grains. The spacing of subgrain boundaries and their misorientations were measured along transects in grains (Fig. 6). Although subgrain boundaries are similarly spaced between differently oriented grains, misorientations of subgrain boundaries show significant orientation dependence of the host grain. The subgrain boundaries in B-grains generally have small misorientations (<3°; Fig. 6a). On the other hand, those in W-grains have

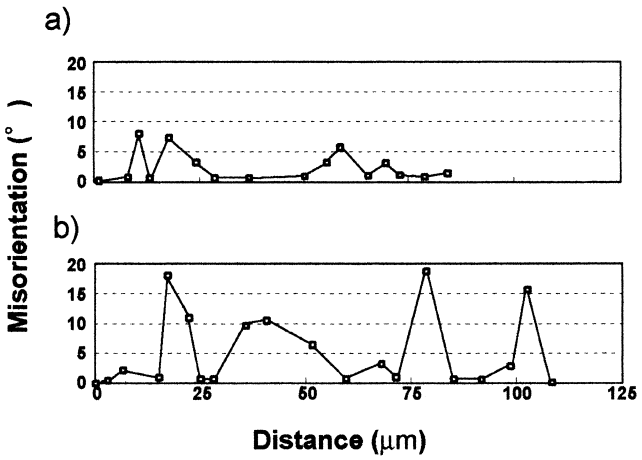

Fig. 6. Misorientations and spacings of subgrain boundaries along transects of (a) B-grain and (b) W-grain.

larger misorientations. Some boundaries with higher than 15° boundary often develop in W-grains, and in this case they are no longer regarded as subgrains but as recrystallized grains (Fig. 6b).

4.3. Intra-granular misorientations

When several potential slip systems with the same critical resolved shear stress are available, the relative ease of slip on a certain slip system can be quantitatively expressed by the Schmid factor. Therefore we investigated the orientation dependence of the magnitude of intra-granular misorientation as a function of the Schmid factor of the host grain, assuming simple shear. According to Law et al. (1990), the Schmid factor for the simple shear kinematic framework is expressed as:

$$Sss = \cos\varphi_1 \cos\alpha_3 + \cos\alpha_1 \cos\varphi_3 \quad (2)$$

where α_1 and α_3 are the angles that the potential slip plane normal makes with the bulk shear direction and the bulk shear plane normal, respectively; and φ_1 and φ_3 are the angles that the potential slip direction lying within the slip plane makes with the bulk shear direction and the bulk shear plane normal, respectively. In this study, the foliation plane normal Z is assumed to be shear plane normal and the lineation direction X the shear direction. The potential slip plane normal and slip direction of a grain have been defined by the mean values of all the measurement points in the grain.

In Fig. 7, the mean intra-granular misorientations (including two mean intra-domain misorientations) of differently oriented grains (and domains) are plotted as a function of *Sss* for the prism$\langle a \rangle$ slip system. W-grains are clustered around *Sss* value less than 0.55, while *Sss* of B-grains are generally higher than 0.75. There is a distinct gap of magnitude of misorientation between these *Sss* clusters. The mean misorientations in the *Sss* value higher than 0.75 (B-grains) are very low, ranging from 1 to 4°. Misorientations in the W-grains and domains (low *Sss* less than 0.55)

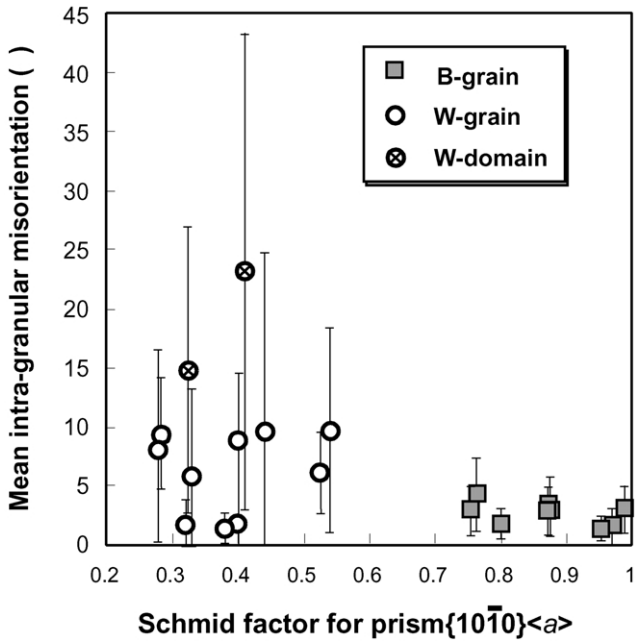

Fig. 7. The intra-granular misorientations of differently oriented grains plotted as a function of the Schmid factor *Sss* for prism{10$\bar{1}$0}⟨*a*⟩ slip, assuming simple shear on the *XY* plane and *X* direction. Each point indicates the mean value of 15–50 misorientations between neighboring measurement points in a grain. The standard deviations are also shown.

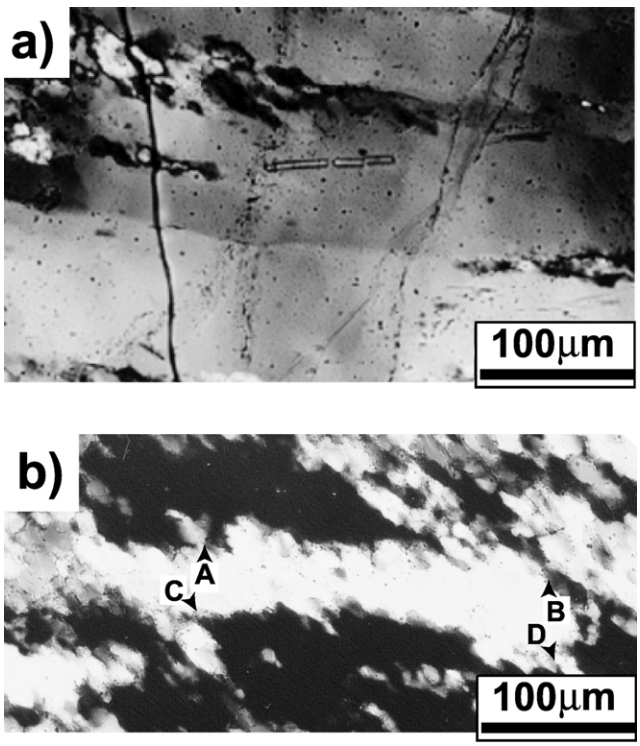

Fig. 8. Optical micrographs (crossed polarizers) showing examples of typical grain boundary shapes. (a) Smooth boundary developed between two B-grains. Misorientation angle is 7°. (b) Highly serrated grain boundary between W- and B-grains. Misorientation angle is 88°. A–B and C–D denote boundary segments used for the curvature analysis (see text and Fig. 9).

are spatially inhomogeneous and mostly around 10°, with large standard deviations. In W-grains, small mean misorientations are sometimes found in the core portion, while large mean misorientations are observed particularly in the vicinity of grain boundaries and inside of kink bands.

4.4. Grain boundary curvature distribution

Examples of representative grain boundary shapes are shown in Fig. 8. Straight or smoothly curved boundaries (Fig. 8a) often develop between two similarly oriented B-grains. On the other hand, significantly serrated grain boundaries frequently develop around W-grains with large intra-granular misorientations (Fig. 8b). Around these boundaries, equant small grains are often observed.

Morphological features of serrated grain boundaries between W- and B-grains have been investigated by means of the grain boundary curvature distribution (Figs. 8b and 9, Appendix 1 and 2). For the curvature analysis, we have defined the senses convexing inward and outward from a W-grain as negative and positive, respectively. Here two representative grain boundary curvature profiles (Fig. 9) are described in detail. The boundary A–B (A–B in Figs. 8b and 9a) is characterized by the sporadic occurrence of large negative curvatures and positive segments of small curvatures (Fig. 9b). This curvature profile reflects the feature of grain boundary serration with cusps sharply pulled into the side of W-grain and gently curved bulges whose centers of curvature are placed in the W-grain. On the other hand, the boundary C–D (C–D in Figs. 8b and 9a) shows, on the whole, small curvatures, and there is no significant difference between curvature distributions for negative and positive senses (Fig. 9c).

We have focused on the differences between the negative and positive curvature distributions and compared their frequency *N*, the absolute average value *Av* and the standard deviation *Sd* for all analyzed grain boundaries (Figs. 8b and 9, Appendix 1 and 2). In Fig. 10, the ratios for each statistical value show one-sided distributions. Although about 70% of the data of $Av(-)/Av(+)$, $Sd(-)/Sd(+)$ and $N(-)//N(+)$ cluster around one, implying no distinct difference between the negative and positive senses as for boundary C–D (Fig. 9c), about 30% show $N(-)/N(+)$ smaller than one, and $Av(-)/Av(+)$ and $Sd(-)/Sd(+)$ larger than one, meaning a predominance of $N(+)$, $Av(-)$ and $Sd(-)$, respectively, represented by A–B (Fig. 9b).

The length between neighboring crest points of serrated grain boundaries along an axis normal to the fluctuation direction of serration has been measured. The length between neighboring crest points range from 0 to 20 μm with an average value of 8.1 μm (Fig. 11a). The distribution of these lengths is comparable with the diameters of short axes of small equant recrystallized grains and subgrains observable by optical microscopy, which range from 0 to 16 μm with an average value of 7.9 μm (Fig. 11b).

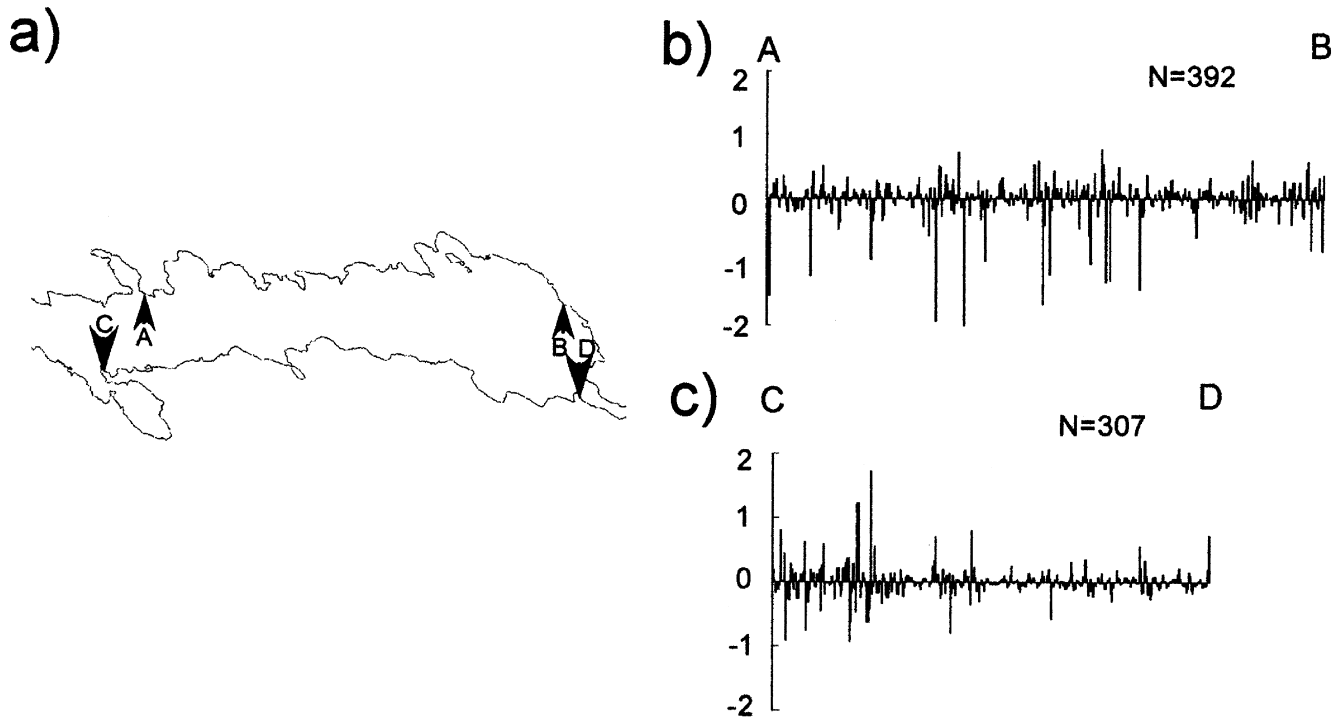

Fig. 9. (a) The trace of the serrated grain boundary shown in Fig. 8b. (b) Curvature profile of boundary segment A–B. (c) That of segment C–D. *N*: Number of points at which grain boundary curvature was calculated.

5. Discussion

It is reasonable to consider that the nuclei of new grains were originally strain free, and therefore they could grow rapidly, consuming more highly deformed old grains. However, since they deform as they grow, the growth rate would decrease with increasing number of dislocations in the new grains. It has been shown experimentally that the free dislocation density saturates quickly in the early stages of deformation under conditions where recovery processes effectively operate. Kirby and McCormick (1979) reported that the dislocation density in quartz becomes independent of strain after only a few percent of deformation. Consequently the difference in dislocation density between new and old grains would be reduced. After dislocations multiplied to a critical density, excess dislocations would annihilate each other or form subgrain boundaries. It has been also known that the spacing of subgrain boundaries decreases with strain in the early stage of deformation and reaches a steady state rapidly. Sakai and Ohashi (1990) demonstrated for hot-deformed nickel that subgrain size reached a steady state at about 50% of the peak stress strain,

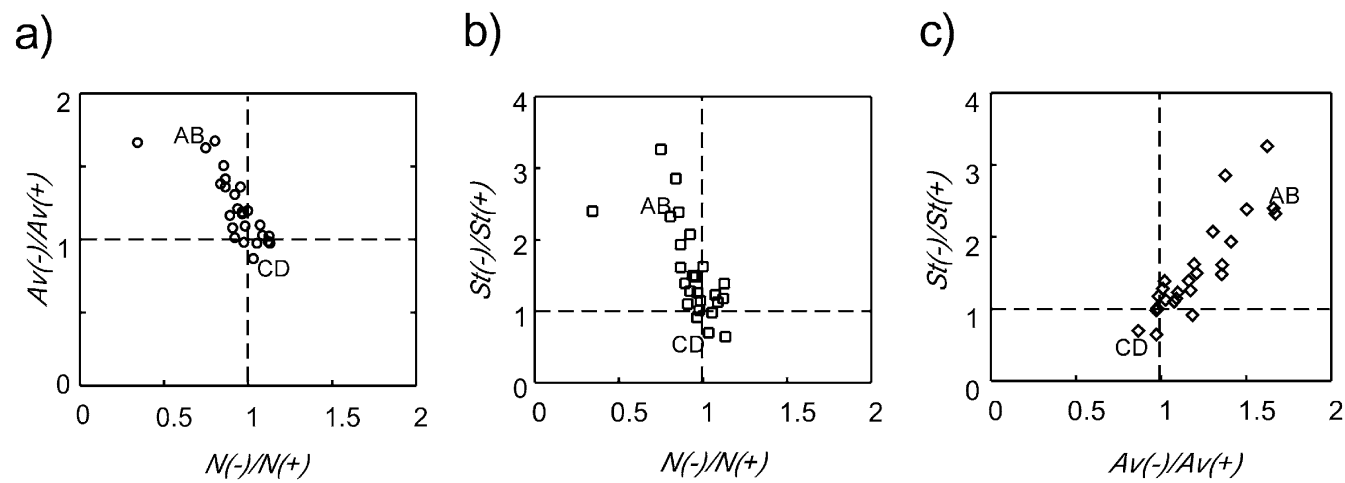

Fig. 10. Diagrams showing the difference of curvature distribution between negative (−) and positive (+) senses for 25 serrated grain boundaries. (a) The absolute of average (*Av*) are plotted as a function of frequency (*N*). (b) Standard deviation (*Sd*) of each boundary is plotted as a function of frequency (*N*). (c) The relation between *Sd* and *Av* are also shown.

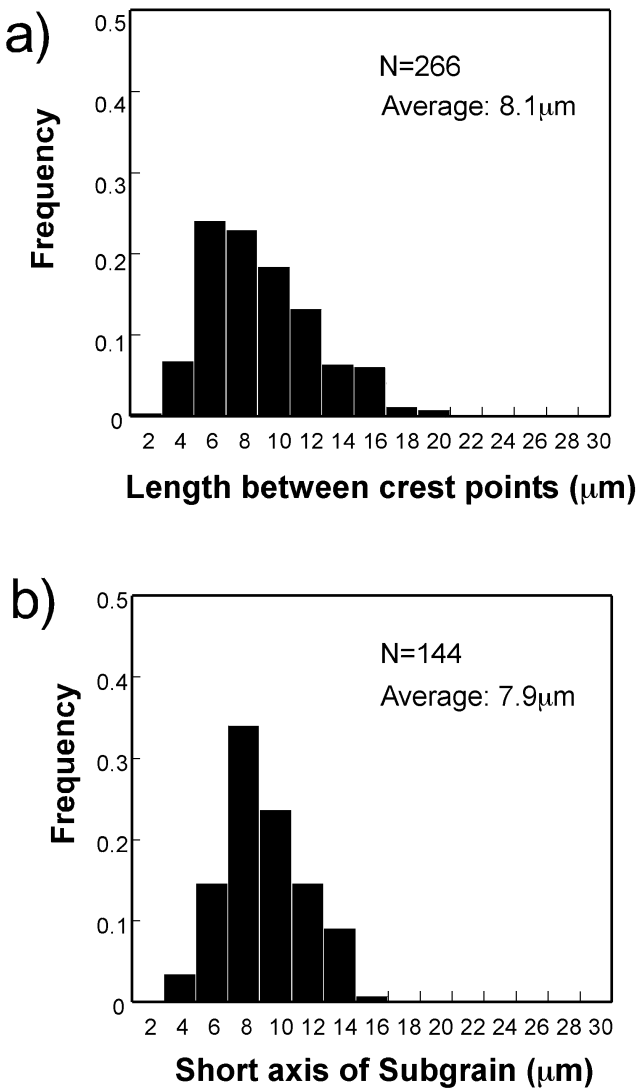

Fig. 11. (a) Frequency distribution of length between crest points of serrated grain boundaries along an axis normal to the fluctuation direction of serration. (b) Frequency distribution of the diameters of short axes of subgrains and equant small recrystallized grains.

at which the magnitude of imposed strain is about 10%. Karato et al. (1980) showed in a high-temperature experiment of olivine single crystals that the dislocation density reached first a steady state, followed by subgrain formation, before dynamic recrystallization occurred. In the present sample, dislocation density and subgrain boundary spacing are of the same order of magnitude in B and W-grains (10^8 cm^{-2} orders and 6 μm, respectively). Therefore, it can be considered that dislocation density and subgrain boundary spacing of most of the grains had already reached steady state, and they would only be subject to an increase of misorientation of subgrain boundaries with further deformation. In fact, only the mean intra-granular misorientations are notably different: generally higher than 10° in W-grains and less than 3° in B-grains. This large gap of mean intra-granular misorientations suggests a difference of stored strain between W- and B-grains.

Grain boundary morphologies in the present sample have been interpreted in relation with intra-granular strain. It has been shown that grain boundaries between two B-grains tend to be smooth. Since there is no large discontinuity of elasticity between both sides of a low angle boundary, and B-grains generally have low intra-granular misorientations, significant local heterogeneity of strain does not occur either across or along the boundary between two B-grains. This could be a reason why boundaries between two B-grains maintain smooth boundary shapes. For W-grains, the wide spread of mean intra-granular misorientations and pervasive development of core and mantle structures indicates that strain was heterogeneously distributed, particularly localized in vicinities of grain boundaries. These localized highly strain portions may have been connected with each through network and resulted in the development of microshear zones like those reported by Herwegh and Handy (1996) in their simple shear experiments for a quartz analog. Many boundaries between W- and B-grains are intensely serrated. We have demonstrated that the morphological features of these serrated boundaries are effectively represented by the grain boundary curvature distribution. The serrations of these grain boundaries have a characteristic length, which is governed by the spacing of subgrain boundaries developed in the grain. Furthermore, making a comparison between negative and positive curvature distributions, we have identified a common morphological feature of serrated grain boundaries as consisting of sharp cusps pointing inside W-grain and gently curved segments between cusps bowing out, which is typically represented by the boundary A–B (Fig. 9b). The boundary cusps in the present sample appear to have developed through subgrain boundary interfacial energy (tension). Here we will evaluate the difference of subgrain boundary energy between W- and B-grains. Read and Shockley (1950) estimated the grain boundary energy E of symmetric low angle tilt boundary per unit area as:

$$E = \mu b/4\pi(1-\nu)\bullet\theta(A_0 - \ln\theta) \quad (3)$$

where θ is the misorientation angle, μ and ν are shear modulus and Poisson's ratio, respectively. A_0 is a term related to the dislocation core energy:

$$A_0 = 1 + \ln(b/r_0) + 4\pi(1-\nu)/\mu b^2 \bullet E_0 \quad (4)$$

where r_0 is the radius of the dislocation core, E_0 is the core energy. Eq. (3) shows that the boundary energy increases with higher misorientation angle θ. Using Eq. (3) with the values: $|b| = d(11\bar{2}0) = 4.9$ Å, $r_0 = b$ (e.g. Poirier, 1985; Wintsch and Dunning, 1985), $\mu = 43.6$ GPa and $\nu = 0.026$ (for 386 °C; Ohno, 1995) and neglecting the unknown term for the core energy in Eq. (4), the mean subgrain boundary energies E are estimated to be 0.28 J m^{-2} for W-grains ($\theta = 10°$) and 0.15–0.2 J m^{-2} for B-grains ($\theta = 2$–$3°$). The estimated subgrain boundary energy in W-grains corresponds to the maximum value and is about 1.5–2 times larger than in B-grains. A large gradient of subgrain

boundary energy between B- and W-grains could control the grain boundary morphology. The cusps pointing inside of the grain with high intra-granular misorientation (W-grains) would be preferentially developed at the site where subgrain boundaries meet grain boundaries.

As shown in the curvature profile of boundary C–D (Fig. 9c), some W-grain boundaries do not exhibit an obvious asymmetric pattern in the serration form (i.e. ratios for each statistical value are around one in Fig. 10). It is probably due to the sectioning effect (Urai et al., 1986). This effect would make the front of cusps spreading sideways in order to reduce total grain boundary energy, and result in cutting off the bulges from the boundary. Presence of small equant W-grains decorating serrated grain boundaries, which seem to have been left behind by the original grain boundary, is evidence for the operation of this process. Both subgrain boundary tension and grain boundary sectioning effectively make a grain boundary migrate inward to W-grains. Consequently, consumption of W-grains by B-grains would gently proceed even under the condition when the gradient of free dislocation density between W- and B-grains is small. Therefore the asymmetric feature of boundary morphology represented in the curvature distribution is useful for predicting the grain boundary migration direction.

However, there is an inconsistency in the inferred migrating direction between the present study of quartz and the prevailing model for strain-induced grain boundary migration (e.g. Bailey and Hirsch, 1962; Roberts et al., 1979). In the model, grain boundary bulges are predicted to be convex in the migrating direction due to the dislocation density gradient across the boundary, which is opposite to our case. In the present sample, however, since the difference in dislocation density between growing and consumed grains is small, the bulging of grain boundaries towards the consumed grains may not occur. However, a large difference of mean subgrain boundary misorientation between growing and consumed grains generates an opposite sense of grain boundary curvature distribution, as described above.

We interpret that the present sample represents transient microstructures in modifying original microstructures that developed under greenschist facies conditions by those of lower amphibolite facies conditions. This may be associated with the change of dominantly activated slip systems from basal$\langle a\rangle$ to rhomb$\langle a\rangle$ and prism$\langle a\rangle$.Alternatively, the microstrucure may be representative of a steady state at intermediate conditions between greenschist facies and lower amphibolite facies. Steady state microstrucures require that each orientation component in the aggregate consist of various generations from strain free to highly deformed grains. It means that W-grains must also consume B-grains, at least partially. We have provided substantial evidence for consumption of W-grains by B-grains through intra-granular strain and grain boundary morphology analyses, but never found evidence for the opposite. Therefore, the former interpretation is preferred.

Since B-grains are thought to be favorably oriented for operation of easy slip systems (rhomb$\langle a\rangle$ and prism$\langle a\rangle$), it can be interpreted that the grains favorably oriented for deformation selectively increased their volume fraction. They did this by replacing unfavorably oriented grains by boundary migration rather than the lattice rotation associated with dislocation gliding under the constraint of surrounding grains (Lister et al., 1978). This conclusion is consistent with previous studies of quartz analog experiments (Herwegh and Handy, 1996; Herwegh et al., 1997) and a simulation of deformation and dynamic recrystallization with the viscoplastic self-consistent theory and comparison with a naturally deformed quartzite of amphibolite facies grade from the Central Alps (Takeshita et al., 1999).

6. Conclusions

We have analyzed stored strains and grain boundary morphologies in sheared quartz aggregates in which both subgrain rotation and grain boundary migration pervasively operate, and arrived at the following conclusions:

(1) Grains favorably oriented for operation of $\{10\bar{1}0\}\langle 1120\rangle$ and $\{10\bar{1}1\}\langle 11\bar{2}0\rangle$ slip systems grew at the expense of those favorably oriented for $(0001)\langle 11\bar{2}0\rangle$ slip. Dislocation density and spacing of subgrain boundaries are similar in magnitude in differently oriented grains (10^8 cm^{-2} orders and 6 μm, respectively). However, the mean intra-granular misorientation is quite different in the consumed and growing grains (higher than 10° and less than 3°, respectively). Subgrain boundary energies of consumed grains are estimated to be approximately 1.5–2 times larger than those of growing grains, assuming symmetric tilt boundaries.

(2) The shapes of the boundaries between growing grains tend to be sharp or smoothly curved. By contrast serrated grain boundaries often develop in highly deformed grains. Grain boundary shapes were characterized by means of the curvature distribution. Serration of a grain boundary is controlled by the misorientations and spacing of subgrain boundaries developed in the grain. We have demonstrated that serrated grain boundaries have a common asymmetric pattern in curvature distribution, and this morphological feature can be used for determining the direction of grain boundary migration.

Acknowledgements

We would like to thank Yanxia Xie, John Donovan and Timothy Teague for their help with the EBSP measurements in Berkeley. We are grateful to Jun-Ichi Ando for arranging TEM experiments at Hiroshima University. We also wish to

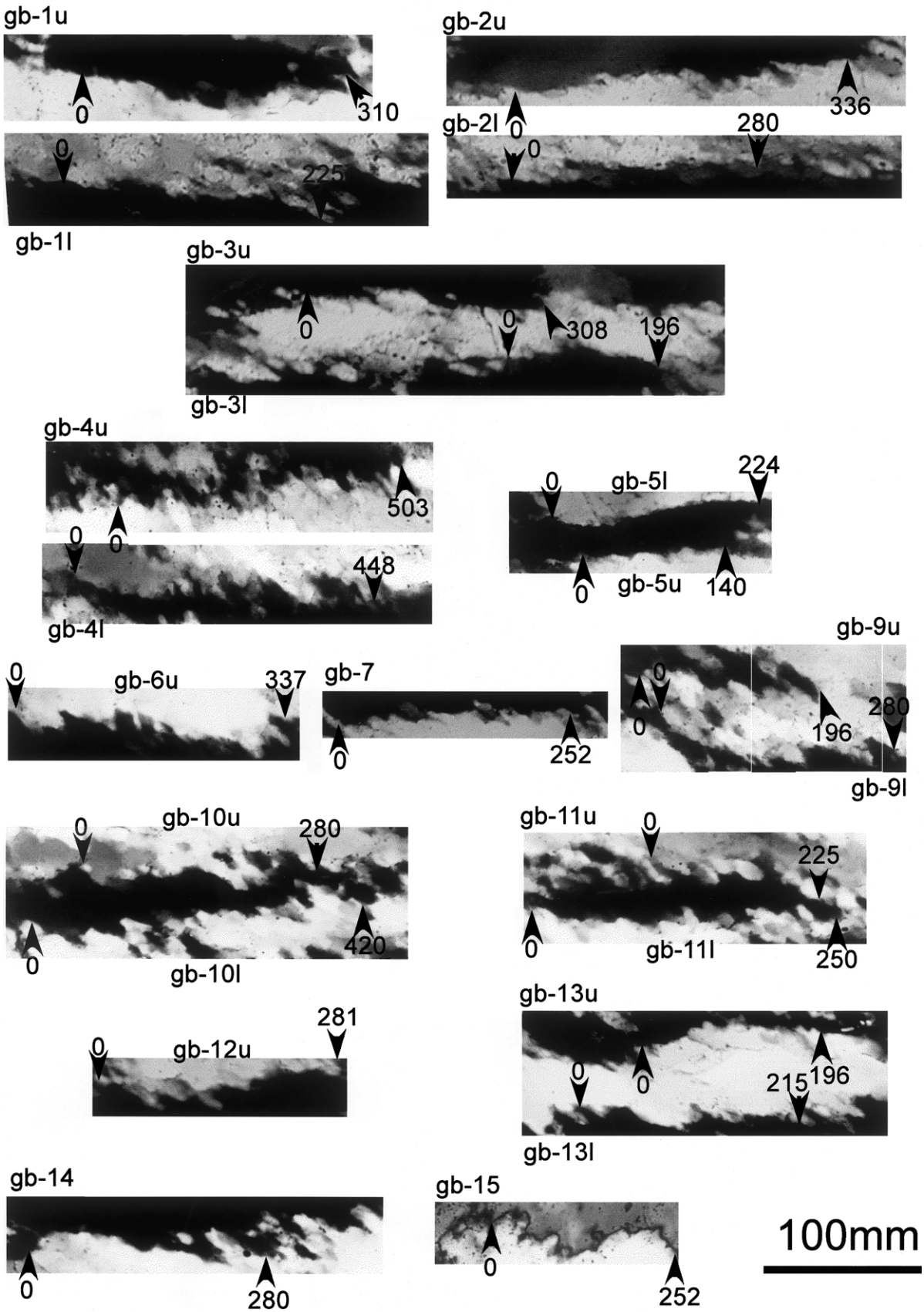

Fig. A1. Serrated grain boundaries used for grain boundary curvature distribution analysis. Darker and brighter sides correspond to B- and W-grains, respectively. Segments between arrowheads were analyzed. The arrowheads with zero and a larger number are pointing at the left and right ends of a histogram in Fig. A2, respectively.

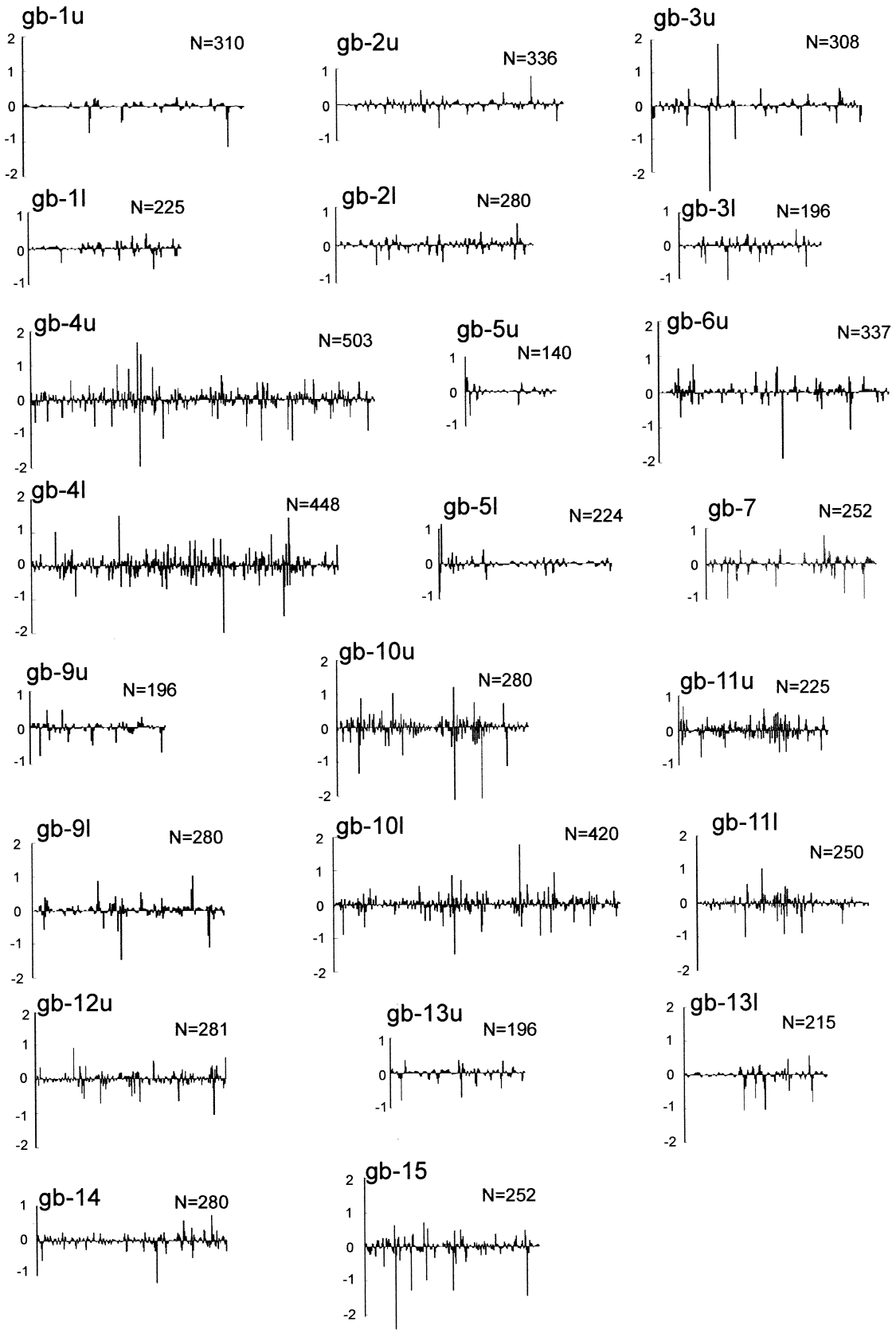

Fig. A2. Curvature profiles of grain boundary segments shown in Fig. A1. Note that the senses convexing inward and outward from a W-grain are defined as negative and positive, respectively. *N*: Number of points at which grain boundary curvature was calculated.

thank Kyuichi Kanagawa, Tomoo Katsura and Akira Yoneda for their useful comments. The original version of the manuscript was much improved by the reviews of Marco Herwegh and Geoffrey E. Lloyd and editorial handling of Joao Hippertt. This work is supported by the Science research grant (B)-2 09440188 from JSPS to Tomoo Katsura. H.-R. Wenk, is appreciative for JSPS support during a visit to Japan.

Appendix

See Fig. A1 and A2.

References

Bailey, J.E., Hirsch, R.B., 1962. The recrystallization process in some polycrystalline metals. Proceedings of the Royal Society A267, 11–30.

Bocher, Ph., Jonas, J.J., 1999. Characteristics of nucleation and growth during the dynamic recrystallization of a 304 stainless steel. In: Sakai, T., Suzuki, H.G. (Eds.), Proceedings of ReX'99. The 4th International Conference on Recrystallization and Related Phenomena, pp. 25–36.

de Bresser, J.H.P., Peach, C.J., Reijs, P.J., Spiers, C.J., 1998. On dynamic recrystallization during solid state flow: effects of stress and temperature. Geophysics Research Letter 25, 3457–3460.

de Bresser, J.H.P., Ter Heege, J.H., Spiers, C.J., 2000. Grain size reduction by dynamic recrystallization: can it result in major rheological weakening? International Journal of Earth Science 90, 28–45.

Bunge, H.-J., 1965. Zur Darstellung allgemeiner Texturen. Zeitschrift fur Metallkunde 56, 872–874.

Dell'Angelo, L.N., Tullis, J., 1989. Fabric development in experimentally sheared quartzites. Tectonophysics 169, 1–21.

Dillamore, I.L., Morris, P.L., Smith, C.J.E., Hutchinson, W.B., 1972. Transition bands and recrystallization in metals. Proceedings of Royal Society of London A329, 405–420.

Doherty, R.D., 1974. The deformation state and nucleation of recrystallization. Metal Science 348, 132–142.

Doherty, R.D., 1997. Recrystallization and texture. Progress in Material Science 42, 39–58.

Drury, C.K., Urai, J.L., 1990. Deformation-related recrystallization processes. Tectonophysics 172, 235–253.

Garcia Celma, A., 1982. Domainal and fabric heterogeneities in the Cap de Creus quartz mylonites. Journal of Structural Geology 4, 443–455.

Gleason, G.C., Tullis, J., Heidelbach, F., 1993. The role of dynamic recrystallization in the development of lattice preferred orientations in experimentally deformed quartz aggregates. Journal of Structural Geology 15, 1145–1168.

Herwegh, M., Handy, M.R., 1996. The evolution of high-temperature mylonitic microfabrics: evidence from simple shearing of a quartz analogue (norcamphor). Journal of Structural Geology 18, 689–710.

Herwegh, M., Handy, M.R., Heilbronner, R., 1997. Temperature- and strain rate-dependent microfabric evolution in monomineralic mylonite: evidence from in situ deformation of norcamphor. Tectonophysics 280, 83–106.

Hobbs, B.E., 1968. Recrystallization of single crystals of quartz. Tectonophysics 6, 359–401.

Hornborgen, E., 1987. Fractal analysis of grain boundaries in hot-worked poly-crystals. Zeitschrift fur Metallkunde 78, 622–625.

Hughes, D.A., 1999. Dislocations of low and high angle boundaries in deformed metals. In: Sakai, T., Suzuki, H.G. (Eds.), Proceedings of ReX'99. The 4th International Conference on Recrystallization and Related Phenomena, pp. 111–118.

Hughes, D.A., Chrzan, D.C., Liu, Q., Hansen, N., 1998. Scaling of misorientation angle distributions. Physical Review Letter 81, 4664–4667.

Humphreys, F.J., Hatherly, M., 1995. Recrystallization and Related Annealing Phenomena, Pergamon, Oxford.

Jones, A.R., 1978. Grain boundary phenomena during the nucleation of recrystallization. In: Haessener, F., (Ed.), Recrystallization of Metallic Materials, Rieder Verlag, Stuttgart, pp. 379–425.

Karato, S.-I., Toriumi, M., Fujii, T., 1980. Dynamic recrystallization of olivine single crystals during high-temperature creep. Geophysical Research Letter 7, 649–652.

Kirby, S.H., McCormick, J.W., 1979. Creep of hydrolytically weakened synthetic quartz crystals oriented to promote $\{\bar{2}110\}\langle 0001\rangle$ slip: a brief summary of work to date. Bulletin of Mineralogy 120, 124–137.

Koshiya, S., 1987. Development of mylonite in the Hatakawa shear zone, Northeast Honshu, Japan. Ph.D. thesis, Tohoku University.

Koshiya, S., 1988. Quartz *c*-axis fabric and microstructure in mylonite. An application to the Hatakawa shear zone. Journal of the Tectonic Research Group of Japan 33, 13–32.(in Japanese with English abstract).

Kruhl, J.H., Nega, M., 1996. The fractal shape of sutured quartz grain boundaries: application as a geothermometer. Geologische Rundschau 85, 38–43.

Kubo, K., Yanagisawa, Y., Yoshioka, T., Yamamoto, T., Takizawa, F., 1990. Geology of the Haramachi and Omika district. With Geological Sheet Map at 1:50,000, Geological. Survey of Japan (in Japanese with English abstract).

Law, R.D., Schmid, S.M., Wheeler, J., 1990. Simple shear deformation and quartz crystallographic fabric: a possible natural example from the Torridon area of NW Scotland. Journal of Structural Geology 12, 29–45.

Lister, G.E., Snoke, A.W., 1984. *S–C* mylonites. Journal of Structural Geology 6, 617–638.

Lister, G.E., Paterson, M.S., Hobbs, B.E., 1978. The simulation of fabric development in plastic deformation and its application to quartzite: the model. Tectonophysics 45, 107–158.

Lloyd, G.E., Freeman, B., 1991. SEM electron channeling analysis of dynamic recrystallization in quartz grain. Journal of Structural Geology 8, 945–953.

Lloyd, G.E., Freeman, B., 1994. Dynamic recrystallization of quartz under greenschist condition. Journal of Structural Geology 16, 867–881.

Mawer, C.K., Fitz Gerald, J.D., 1993. Microstructure of kink band boundaries in naturally deformed Cewings Range quartzite. In: Boland, J.N., Fitz Gerald, J.D. (Eds.), Defects and Processes in the Solid State: Geoscience Applications. The McLaren Volume, Elsevier, Amsterdam, pp. 49–67.

McLaren, A.C., 1991. Transmission Electron Microscopy of Minerals and Rocks, Cambridge University Press, Cambridge.

Mino, K., Fukuoka, C., Yoshizawa, H., 2000. Evolution of intragranular misorientation during plastic deformation. Journal of the Japan Institute of Metals 64, 50–55 (in Japanese with English abstract).

Nishikawa, O., Takeshita, T., 2000. Progressive lattice misorientation and microstructural development in quartz veins deformed under sub-greenschist conditions. Journal of Structural Geology 22, 259–276.

Ohno, I., 1995. Temperature variation of elastic properties of α-quartz up to the α–β transition. Journal of Physics of the Earth 43, 157–169.

Otsuki, K., Ehiro, M., 1992. Cretaceous left-lateral faulting in Northeast Japan and its bearing on the origin of geologic structure of Japan. Journal of the Geological Society of Japan 98, 1097–1112.(in Japanese with English abstract).

Pauli, C., Schmid, S.M., Heilbronner, R.P., 1996. Fabric domains in quartz mylonites: localized three-dimensional analysis of microstructure and texture. Journal of Structural Geology 18, 1183–1203.

Poirier, J.-P., 1985. Creep of Crystals. High-temperature Deformation Processes in Metals, Ceramics and Minerals, Cambridge University Press, Cambridge.

Poirier, J.-P., Nicolas, A., 1975. Deformation induced recrystallization due

to progressive misorientation of subgrains, with special reference to mantle peridotites. Journal of Geology 83, 707–720.

Randle, V., 1993. The Measurement of Grain Boundary Geometry, IOP Publishing, Bristol.

Read, W.T., Shockley, W., 1950. Dislocation models of crystal grain boundaries. Physical Review 78, 275–289.

Roberts, W., Boden, H., Ahlbom, B., 1979. Dynamic recrystallization kinetics. Metal Science 13, 195–205.

Saiki, K., 1997. Morphology and simulation of solid state rounding process. Geophysical Research Letters 24, 1519–1522.

Sakai, T., Ohashi, M., 1990. Dislocation substructures developed during dynamic recrystallization in polycrystalline nickel. Materials Science and Technology 6, 1251–1257.

Shigematsu, N., Yamagishi, H., 2002. Quartz microstructures and deformation conditions in the Hatagawa shear zone, north-eastern Japan. The Island Arc 11, 45–60.

Stipp, M., Stüitz, H., Heilbronner, R., Schmid, S.M., 2002a. The eastern Tonale fault zone: A "natural laboratory" for crystal plastic deformation of quartz over a temperature range from 250 to 700 C. Journal of Structural Geology 24, 1861–1884.

Stipp, M., Stüitz, H., Heilbronner, R., Schmid, S.M., 2002b. Dynamic Recrystallization of quartz: Correlation between Natural and Experimental Conditions. In: de Meer, S., Drury, M.R., de Bresser, J.H.P., Pennock, G.M. (Eds.), Deformation Mechanisms, Rheology and Tectonics: Current Status and Future Perspectives. Geological Society, London, Special Publications. 200, 171–190.

Takahashi, M., Nagahama, H., Masuda, T., Fujimura, A., 1998. Fractal analysis of experimentally, dynamically recrystallized quartz grains and its possible application as a strain rate meter. Journal of Structural Geology 20, 269–275.

Takeshita, T., Wenk, H.-R., 1988. Plastic anisotropy and geometrical hardening in quartzites. Tectonophysics 149, 345–361.

Takeshita, T., Wenk, H.-R., Lebensohn, R., 1999. Development of preferred orientation and microstructure in sheared quartzite: comparison of natural data and simulated results. Tectonophisics 312, 133–155.

Tanaka, M., Iizuka, H., 1991. Characterization of grain boundaries by fractal geometry and creep-rupture properties of heat- resistant alloys. Zeitschrift fur Metallkunde 82, 422–447.

Tomé, C.N., Wenk, H.-R., 1999. Modeling dynamic recrystallization of geologic aggregates. In: Sakai, T., Suzuki, H.G. (Eds.), Proceedings of ReX'99. The 4th International Conference on Recrystallization and Related Phenomina, pp. 665–670.

Toriumi, M., 1989. Microstructures of regional metamorphic rocks. In: Karato, S., Toriumi, M. (Eds.), Rheology of Solids and of the Earth, Oxford University Press, New York, pp. 319–337.

Trimby, P.W., Prior, D.J., Wheeler, J., 1998. Grain boundary hierarchy development in a quartz mylonite. Journal of Structural Geology 20, 917–935.

Trozschel, J., Pantleon, M., Haberjahn, M., Klimanek, P., 1997. Formation of dislocation in aluminum single crystals during hot-compression. Materials Science and Engineering A234-236, 842–845.

Tsurumi, J., Hosonuma, H., Kanagawa, K., 2003. Strain localization due to a positive feedback of deformation and myrmekite-forming reaction in granite and aplite mylonites along the Hatagawa shear zone of NE Japan. Journal of Structural Geology 25, 557–574.

Urai, J.L., Means, W.D., Lister, G.S., 1986. Dynamic recrystallization of minerals. In: Hobbs, B.E., Heard, H.C. (Eds.), Mineral and Rock Deformation: Laboratory Studies. The Paterson Volume, Geophysical Monograph 36, American Geophysical Union, Washington, DC, pp. 161–199.

Watanabe, I., Sotozaki, Y., Gorai, M., 1953. Geology of the northeastern border district of northern Abukuma plateau. Science Reports of the Tokyo Education University 2, 69–78 (in Japanese with English abstract).

Wenk, H.-R., 1994. Preferred orientation patterns in deformed quartzites. In: Heaney, P.J., Prewitt, C.T., Gibbs, G.V. (Eds.), Reviews in Mineralogy 29, Silica Minerals, Mineralogical Society of America, Washington, DC, pp. 177–208.

Wenk, H.-R., Matthies, S., Donovan, J., Chateigner, D., 1997. BEARTEX: a Windows based program for quantitative texture analysis. Journal of Applied Crystals 31, 262–269.

Wenk, H.-R., Donovan, J.J., Xie, Y., Johnson, G.C., Toker, E., 1999. Texture analysis with a digital SEM-EBSD system. In: Szpunar, J.A., (Ed.), Proceedings of International Conference on Textures of Materials, NRC Research Press, Ottawa, pp. 235–240.

Wheeler, J., Prior, D.J., Jiang, Z., Speiss, R., Trimby, P.W., 2001. The petrological significance of misorientations between grains. Contribution of Mineralogy and Petrology 141, 109–124.

Wintsch, P., Dunning, J., 1985. The effect of dislocation density on the aqueous solubility of quartz and some geologic implications: a theoretical approach. Journal of Geophysical Research 90, 3649–3657.

Yoshizawa, H., Nakashiro, M., Kihara, S., Nakagawa, Y., 1995. Strain measurement by intra-granular dislocation analysis in creep of 2.25Cr–1Mo steel. Tetsu-to-Hagane 81, 53–58 (in Japanese with English abstract).